
Noradrenergic-inspired gain modulation attenuates the stability gap in joint training

Alejandro Rodriguez-Garcia*
Neural Circuits Laboratory, Biosciences Institute
Newcastle University, UK
a.rodriguez-garcia2@newcastle.ac.uk

Anindya Ghosh
Department of Informatics
University of Sussex, UK
anindya.ghosh@sussex.ac.uk

Srikanth Ramaswamy
Neural Circuits Laboratory, Biosciences Institute
Newcastle University, UK
srikanth.ramaswamy@newcastle.ac.uk

Abstract

Recent studies in continual learning have identified a transient drop in performance on mastered tasks when assimilating new ones, known as the stability gap. Such dynamics contradict the objectives of continual learning, revealing a lack of robustness in mitigating forgetting, and notably, persisting even under an ideal joint-loss regime. Examining the stability gap within this idealized joint training context is critical to isolate it from other sources of forgetting and fully elucidate its underlying mechanisms. We argue that this gap reflects an imbalance between rapid adaptation and robust retention at task boundaries, underscoring the need to investigate mechanisms that reconcile plasticity and stability within continual learning frameworks. Biological brains navigate a similar plasticity–stability dilemma by operating concurrently on multiple timescales, leveraging neuromodulatory signals to modulate synaptic plasticity. However, artificial networks lack native multitimescale dynamics, and although optimizers like momentum-SGD and Adam introduce implicit timescale regularization, they still exhibit stability gaps. Inspired by locus coeruleus-mediated noradrenergic bursts, which transiently enhance neuronal gain under uncertainty to facilitate sensory assimilation, we propose uncertainty-modulated gain dynamics – an adaptive mechanism that approximates a two-timescale optimizer and dynamically balances integration of knowledge with minimal interference on previously consolidated information. We evaluate our mechanism on domain-incremental and class-incremental variants of the MNIST and CIFAR benchmarks under joint training, demonstrating that uncertainty-modulated gain dynamics effectively attenuate the stability gap. Finally, our analysis elucidates how gain modulation replicates noradrenergic functions in cortical circuits, offering mechanistic insights into reducing stability gaps, and that gain-modulated neural networks can enhance performance in continual learning tasks.

1 Introduction

Biological neural circuits demonstrate lifelong adaptability, continually integrating new information with minimal disruption to established memories [18], [38]. This capability rests on a finely tuned

*Corresponding author.

balance between plasticity and stability, arising from intrinsic multi-timescale dynamics in cortical networks [17], [36], [38]. Gain modulation is a central mechanism supporting this flexibility, whereby a neuron’s responsiveness is scaled without altering its selectivity [5], [18], [33]. While various biological pathways can modulate gain, we focus on its amplification during perceptual integration, which critically depends on locus coeruleus–mediated noradrenergic phasic bursts triggered by environmental uncertainty [5], [17], [33], [39]. Neural networks mimicking this process observe flattened energy landscapes, making network states more accessible and enhanced flexibility during perceptual integration [17], [20], [29], [39].

During the presentation of novel and unexpected events, transient gain boosts have been observed [5], [9], [39]. We hypothesize that these transient gain boosts on neural circuits also induce fast and slow timescales of weight adaptations that facilitate sensory integration with minimal interference. In this way, gain-induced weight dynamics mirror the fast-and-slow paradigm, i.e., when learning a new task, fast weights temporarily enhance performance on previous tasks without disturbing the consolidation of new memories being stored in the slow weights [2] – but achieve even greater efficiency thanks to the flexibility conferred by a flattened energy landscape. Crucial to our point, while gain modulation in biology operates via changes in spiking behavior [29], [31], it can be applied in standard multilayer perceptrons (MLPs) by multiplying each point neuron’s incoming weights with a gain coefficient.

Continual learning (CL) in artificial neural networks aspires to emulate this lifelong adaptability – networks acquire incoming data continuously, without "catastrophically" overwriting the knowledge of past examples [23], [24], [38]. To date, most work in this field has concentrated on mitigating this phenomenon by approximating the ideal joint loss over all previous tasks encountered [23], [28]. However, recent research has pointed out the presence of a stability gap – a transient forgetting of past task knowledge at every task switch and shown that it persists even under ideal joint-training conditions [19], [21]. This brief drop in accuracy impairs the essence of CL, which seeks seamless knowledge accumulation, and raises two questions: (i) does similar transient forgetting occur in neural systems, and (ii) if not, do CL’s learning dynamics diverge from those of biological brains? As a result, efforts are emerging focusing not only on what to optimize, but also on how to optimize [28]. Our research is based on this new approach in CL, where we propose an uncertainty-modulated gain mechanism as an approximated two-timescale optimizer that outperforms two well-established gradient-based optimization techniques – momentum-SGD (MSGD) [4] and Adam [13] optimizers in attenuating stability gaps in the ideal joint-training scenario. The main contributions of our work are:

- We introduce uncertainty-guided gain dynamics to attenuate stability gaps in CL, and analytically show that transient gain boosts induce fast and slow timescales of weight adaptation, effectively approximating classic fast-and-slow weight schemes through implicit multi-timescale regularization.
- We empirically validate our approach on both domain-incremental and class-incremental MNIST (Split MNIST, Rotated MNIST, Permuted MNIST) and CIFAR (Split CIFAR 10, Domain CIFAR-100) benchmarks under ideal joint training, demonstrating a substantial reduction of the stability gap compared to the MSGD and Adam optimizers.
- We link our algorithmic gain bursts to noradrenergic neuromodulation, providing a biologically inspired perspective on how multi-timescale dynamics can mitigate transient forgetting while promoting knowledge acquisition.

2 Related work

Multi-timescale optimizers. Standard multi-layer perceptron architectures lack explicit multiscale dynamics, which makes them hard to optimize effectively with vanilla SGD. To overcome this, MSGD introduced a two-timescale update that maintains an exponentially weighted average of past gradients alongside the current gradient [1], [4]. Adaptive optimizers such as Adam build on this principle by combining first-moment (momentum) and second-moment (variance) estimates to adjust per-parameter learning rates on the fly, coupling rapid responsiveness with step-size normalization for faster, more stable convergence [13]. Interestingly, recent work demonstrated that MSGD could be reparameterized into “fast” and “slow” weight components, where the fast channel adapts quickly but decays, and the slow channel integrates information more stably [22]. Hence, these modern optimizers echo the original fast–slow weight idea of Hinton and Plaut [2], who paired a fast, elastic

weight that decays toward zero with a slow, plastic weight, to temporarily “deblur” old associations (the fast weights take on values that temporarily cancel out the changes in the slow weights caused by the subsequent learning) and thus minimize interference from new learning [2].

Stability gaps in CL. It was not until recently that a study pointed out the conventional evaluation paradigm for AI systems is fundamentally inadequate [21], [28]. Consider a sequence of tasks $\{T_k\}_{k=1}^K$ with corresponding data distributions $\{D_k\}_{k=1}^K$ and let \mathcal{F}_θ denote a model parameterized by θ . Under the traditional task-based evaluation, \mathcal{F}_θ is trained sequentially, updating its parameters θ_k upon completing task T_k , and its performance is measured only immediately after training on T_k has finished [21]. Notably, this task-based evaluation is blind to how a model’s accuracy evolves during training. As an alternative, the continual evaluation strategy measures the performance of \mathcal{F}_θ every ρ training iterations while learning task T_k [21]. Surprisingly, continual evaluation revealed stability gaps [19], [21], which have been encountered even in LLMs [32]. These brief accuracy drops undermine the goals of CL by introducing temporary forgetting between tasks and limiting the system’s overall learning capacity. Specifically, this might be especially problematic in safety-critical applications, where even momentary failures can have severe consequences [21], [28]. One may naively attribute the stability gap to imperfect approximations of the joint objective by CL methods. Yet this hypothesis does not hold up as the phenomenon persists even under perfect joint training, where $L_{\text{joint}} = L_{\text{new}} + L_{\text{old}}$ [28], [34]. Hence, this finding implies that the transient performance collapse is not merely an artifact of memory or regularization approximations, but rather emerges from the fundamental dynamics of sequential optimization, underscoring the importance of studying it in the idealized joint-loss setting [34].

Beyond evaluation paradigms and identification of the stability gap, a growing body of work has sought to pinpoint its causes and propose remedies. Hess *et al.* [28] argue that there exists a non-increasing-loss path between θ_{old} and θ_{joint} – suggesting that a continual learner only needs to follow this valley. However, enforcing this trajectory via gradient-projection methods has yielded limited success [28]. In a homogeneous-CIFAR setup, Kamath *et al.* [34] further demonstrates that although such a linear, low-loss path does exist, standard SGD consistently deviates from it at each task transition. Other approaches argue that the stability gap may originate from excessive network plasticity or large losses in the output layer [27]. Successful approaches include temporal ensembling to narrow the gap by reducing prediction variance at task transitions [30] and replacing the standard linear classifier with a nearest-mean classifier head [35]. Interestingly, in this last method, Łapacz *et al.* [35] demonstrates that much of the transient forgetting arises in the final linear classifier. However, to the best of our knowledge, no prior work has adopted a bio-inspired approach to mitigate the stability gap or connected it back to adaptive biological learning.

Neuronal gain modulation. Neuronal gain characterizes the input sensitivity of a neuron and is formally defined as the slope of its input-output transfer function, reflecting the rate at which output firing rates change in response to variations in input current [5], [18], [33]. This property has been extensively investigated in biophysical models of cortical circuits, highlighting the role of gain modulation in adaptive computation [6], [10], [14], [29], [37], and fine-tuning motor responses [16]. Furthermore, theoretical neuroscience works have debated the causal relationship between gain modulation and synaptic plasticity, suggesting a complex interplay [7]. However, despite its biological relevance, gain modulation has received limited attention in artificial learning systems. A recent study has used gain modulation for attentional gating in hierarchical models but only as a fine-tuning step after weight learning, ignoring its interaction with weight updates [40]. Another study used it as an isolated mechanism for adaptive whitening [25] and extended it to multi-timescale whitening by pairing fast gain changes with slower synaptic plasticity [26]; however, their gain modulation was limited to interneurons in a single-layer architecture [25], [26]. Nevertheless, a key theoretical insight is that gain neuromodulation reshapes the energy landscape: noradrenergic input flattens it to enable flexible switching, while cholinergic input deepens it to stabilize memories [17], [20], [29]. Recent recurrent neural network (RNN) work supports this view, showing that uncertainty-driven gain modulation facilitates perceptual switches by propelling the system through high-velocity trajectories [39]. However, in that model, gains were fixed during training and modulated only afterward, limiting interaction with weight updates. We extend this approach by including gain dynamics during learning and applying it to reduce stability gaps in joint-CL.

3 Gain boost as a multi-timescale optimizer

Introducing processing timescales into artificial neural networks provides a principled strategy to reconcile stable, long-term memory consolidation with rapid, context-driven adaptation. The fast-slow weight paradigm exemplifies this principle by maintaining distinct "slow" and "fast" weight components, i.e. $W_{\text{eff}} = w_{\text{slow}} + w_{\text{fast}}$ [2]. This enables networks to swiftly adapt to distribution shifts through transient updates in the fast weights, which rapidly decay toward zero, while simultaneously preserving consolidated knowledge within slow weights [22]. Crucially, this structure minimizes interference between newly acquired information and existing representations [2], making it particularly suitable as a foundation for lifelong learning in artificial systems.

In biological neural circuits, analogous multi-timescale processing occurs through neuromodulatory signals that adjust neuronal gain, thereby altering neuronal responsiveness to incoming stimuli [5], [17], [18]. For instance, during perceptual updating, the noradrenergic system originating from the locus coeruleus transiently boosts neuronal gain to facilitate sensory integration of new incoming stimuli [5], [33], [39]. We propose that this neuronal gain modulation naturally gives rise to a fast-slow learning structure by shaping the effective synaptic weights. Consider a model $y(t) = h(x(t); g(t), w(t))$ and a loss function $L(y(t), T(t))$, where $x(t)$ represents the input at time t , $\{g(t), w(t)\}$ denotes the parameter estimate, $y(t)$ is the output produced by the model, and $T(t)$ is the target. In artificial neural networks (ANNs), we can interpret $w_{ij}(t)$ as the synaptic weights connecting neuron j with neuron i and $g_i(t)$ as the neuronal gain; hence, one can consider an effective weight

$$W_{ij}(t) = g_i(t)w_{ij}(t) \quad (1)$$

Assuming that neuronal gain is shaped by noradrenergic activity, we can distinguish two functional modes of operation: (i) phasic – rapid, high-amplitude bursts of release and (ii) tonic – background level of neuromodulatory release. Sensory prediction errors trigger phasic noradrenaline release, which transiently increases neuronal gain [33]. However, in the absence of prediction errors, neuronal gain tends toward its baseline g_0 , reflecting tonic activity. Therefore, without losing generalizability, we can decompose the effective weight as contributions from these components, i.e.

$$W_{ij}(t) = g_i(t)w_{ij}(t) = g_0w(t) + [g_i(t) - g_0]w_{ij}(t), \quad (2)$$

This decomposition highlights how neuronal gain modulation inherently realizes a two-timescale optimization scheme. The slow component, $w_{ij}^{\text{slow}}(t) = g_0w(t)$, represents the stable synaptic changes associated with tonic neuromodulation. Conversely, the fast component, $w_{ij}^{\text{fast}}(t) = [g_i(t) - g_0]w_{ij}(t)$ dynamically emerges in response to phasic neuromodulatory signals, effectively isolating rapid contextual adaptations from stable memory traces. In other words, transient gain modulation "virtually" decouples the effective synaptic weight updates into slow and fast components, offering an adaptive mechanism to flexibly balance plasticity and stability (Figure 1A).

To illustrate this concept further, following Jones [22], we consider a simplified linear model defined by $y(t) = W_{\text{eff}}(t)x$ with a constant input $x \equiv 1$ to predict a target signal $T(t)$ under the mean square error loss $L = \frac{1}{2}[T(t) - y(t)]^2$. Parameter updates follow standard stochastic gradient descent, while gain dynamics evolve via exponential decay modulated by transient increases in response to contextual surprises. Formally, we can write

$$w(t+1) = w(t) - \alpha \partial_w L, \quad (3)$$

$$g(t+1) = \gamma g(t) + (1 - \gamma)g_0 + \eta H(y), \quad (4)$$

where α is the learning rate, $\gamma < 1$ controls how quickly the gain decays back to its tonic baseline g_0 , and η determines the strength of the phasic bump, driven by the "surprise" signal $H(y)$ which in this case is simplified as the absolute value of the loss gradient, $|\partial_y L|$. Note that these constraints on the gain update mimic noradrenergic release by the locus coeruleus ([39]; see the Appendix for details).

Given that the gradient with respect to synaptic weights can be expressed as:

$$\frac{\partial L}{\partial w} = g(t) \frac{\partial L}{\partial W}, \quad (5)$$

neuronal gain acts explicitly as a plasticity modulator, dynamically scaling the magnitude of learning updates. During phasic increases in neuronal gain, this modulation amplifies synaptic updates, allowing rapid adaptation to novel contexts. Conversely, during tonic baseline activity, it ensures

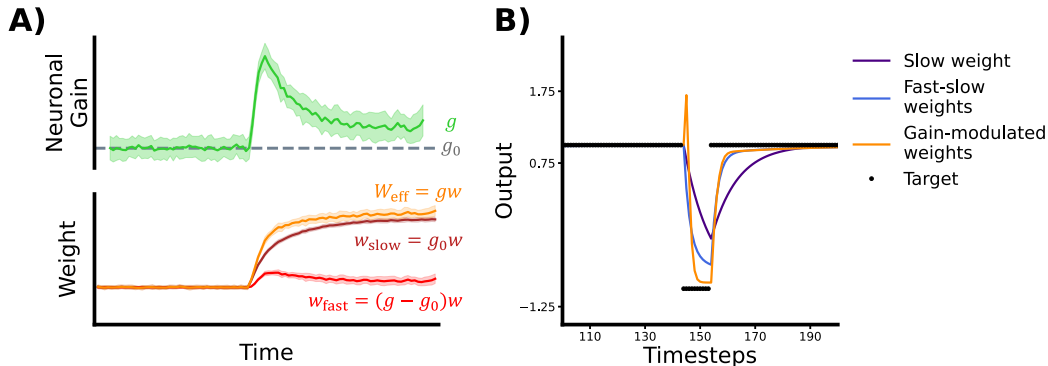


Figure 1: **Simple proof of principle of gain boost approximating to two-timescale optimizer.** A) Schematic of the gain effective weight uncoupling under a gain boost through noradrenergic neuromodulation. Phasic noradrenergic signals transiently increase neuronal gain henceforth decoupling its weights in a fast-slow scheme where: $w_{\text{slow}} = (g(t) - g_0) w(t)$ and $w_{\text{slow}} = g_0 w(t)$. B) We consider the simplified model $y(t) = W_{\text{eff}}(t) x$, with a constant input x to predict a target signal $T(t)$ under the mean square error loss $L = \frac{1}{2} [T(t) - y(t)]^2$. Comparison between the gain modulated (blue) and fast-slow weight (orange) methods. The slashed line reflects the basal model with only the slow component.

stable, incremental learning, thereby minimizing interference with previously consolidated memories. Thus, gain modulation naturally approximates a fast–slow optimization scheme (see the comparison in Figure 1B), effectively mitigating catastrophic forgetting by dynamically balancing rapid adaptation and long-term stability [2].

Interestingly, classical MSGD can be reinterpreted within this framework as implicitly implementing a fast–slow weight separation, where a "fast" component smooths high-frequency noise through an exponentially decaying memory of past gradients [22]. Similarly, Adam optimizer could be viewed through a multi-timescale lens, where its adaptive step-size adjustments reflect a fast-timescale adaptation based on local gradient statistics [13]. However, these conventional optimizers achieve multi-timescale dynamics indirectly through adaptive learning rates, whereas gain modulation emerges directly from biologically inspired neuronal properties. Moreover, biologically realistic gain modulation actively reshapes the network’s energy landscape by transiently flattening it, thereby facilitating smoother transitions between stable attractors corresponding to distinct learned states [20], [29], [39], hence being a promising venue to balance stability and plasticity in both biological and artificial neural circuits.

4 Joint training experiments

We isolate the stability gap from other sources of forgetting by simplifying into a joint training scenario between tasks, as we are focusing on how to optimize and not what to optimize [28], [34]. Our hypothesis is rooted in gain modulation’s ability to both segregate synaptic plasticity into fast and slow adaptation channels and flatten the network’s energy landscape. This dual action should narrow stability gaps between successive tasks and lower test-set loss at contextual changes, together minimizing interference. To test this, we consider a scenario in which a learner F_θ is trained on a sequence of K contexts $\mathcal{C} = \{c_k\}_{k=1}^K$. Each context c_k is a disjoint dataset $\{(\mathbf{x}_j, \tilde{y}_j)\}_{j=1}^N \sim \mathcal{D}_k$. Contexts are presented one after another in an online fashion, with each context trained for a fixed number of iterations I_C ². Since this is a joint-training setup, the model retains access to all data from previous contexts throughout learning.

Noradrenergic uncertainty. Biological and theoretical evidence converge on the necessity of explicitly representing a learner’s uncertainties when interacting with stochastic, non-stationary environments to achieve optimal inference [8], [9], [33]. Noradrenaline has been particularly linked to “unexpected uncertainty,” where its phasic signaling is triggered by sudden increases in environmental variability due to contextual changes [8], [9], [33], [38]. This response injects additional variability

²Due to random sampling, some individual examples may be seen multiple times – especially when the total number of training iterations exceeds the size of the training set.

Algorithm 1 Noradrenergic Gain-Modulated SGD (NGM-SGD)

Require: Dataset sequence $\mathcal{C} = \{c_k\}_{k=1}^K$, where each $c_k = \{(\mathbf{x}_j, \tilde{y}_j)\}_{j=1}^N \sim \mathcal{D}_k$; context iterations I_C ; batch size B ; learning rate $\alpha > 0$; gain-decay $0 < \gamma < 1$; gain-baseline $g_0 \geq 1$; entropy scale $\eta > 0$

- 1: **Initialize:** $\mathbf{W} \leftarrow \mathbf{W}_{\text{init}}$; $g \leftarrow g_{\text{init}}$
- 2: **for** each context $c_i \in \mathcal{C}$ **do**
- 3: **for** iteration $i = 1$ **to** I_C **do**
- 4: $(\mathbf{X}, \tilde{\mathbf{Y}}) \sim \mathcal{D}_k^B$ // mini-batch
- 5: $\boldsymbol{\pi} \leftarrow \text{softmax}(F_{\mathbf{W}}(\mathbf{X}; g))$ // forward pass
- 6: $\mathcal{L} \leftarrow \frac{1}{B} \sum_{j=1}^B \ell(\pi_j, \tilde{y}_j)$ // cross-entropy loss
- 7: $\mathbf{W} \leftarrow \mathbf{W} - \alpha \nabla_{\mathbf{W}} \mathcal{L}$ // SGD update
- 8: $H \leftarrow -\frac{1}{B} \sum_{j=1}^B \sum_l \pi_{j,l} \log \pi_{j,l}$ // uncertainty (entropy)
- 9: $g \leftarrow \gamma g + (1 - \gamma) g_0 + \eta H$ // gain update
- 10: **end for**
- 11: **end for**

into neural and behavioral processes, facilitating rapid adaptation to shifting contexts [17], [20], [39]. Evidence in this regard from Wainstein *et al.* [39], suggests that this form of uncertainty can be quantified as the entropy of the network’s readout, i.e.

$$H(y) = \sum_i \pi_i(y) \log(\pi_i(y)) \quad (6)$$

where $\pi(y)$ denotes the softmax probability distribution of the network’s output. We incorporate this into equation (4) to dynamically modulate neuronal gain, which acts as a forcing function that transiently boosts gain in response to novel or ambiguous stimuli [5], [17], [33]. Consistent with our hypothesis, this will lead to faster knowledge integration with minimal integration. As discussed above, this modulation approximates a two-timescale optimization mechanism (see Equations (3) and (4)). To further formalize this process, we present the pseudo-algorithm in Algorithm 1 and benchmark its performance against standard optimizers such as MSGD and Adam to evaluate whether it offers improved adaptability and reduced interference.

4.1 Methods

Datasets. For our class-incremental learning experiments, we used two standard benchmarks: MNIST [3] and CIFAR-10 [11]. We define Split MNIST and Split CIFAR-10 by dividing each dataset into 5 sequential tasks, each containing a disjoint subset of the 10 target classes [28]. For domain-incremental learning, we considered MNIST [3] and CIFAR-100 [11]. We defined Rotated MNIST with three tasks, each using the full MNIST dataset rotated by a fixed angle: $0^\circ, 80^\circ, 160^\circ$. These angles were chosen to maximize stability gaps while avoiding digit ambiguities, such as confusing 6 and 9 when rotated 180° [21], [28]. We define Permuted MNIST by applying fixed random pixel permutations to each image in the full MNIST dataset [12]. We define Domain CIFAR-100 by organizing tasks according to the coarse semantic categories in CIFAR-100 [28]. Specifically, we constructed three tasks using the superclasses *aquatic mammals*, *fish*, and *flowers*, progressively expanding the visual diversity while keeping the label space consistent.

Setup. We employed continual evaluation with $\rho_{\text{eval}} = 1$ and test on all the testing data of the first task [21]. Batch sizes were chosen as 128 for experiments on the MNIST dataset and 256 for experiments on the CIFAR-10 and CIFAR-100 datasets. Per experiment, the number of iterations per context (I_C) was selected as Permuted MNIST (200), Rotated MNIST (400), Split MNIST (200), Split CIFAR-10 (400), and Domain CIFAR-100 (400). Each experiment was repeated five times with different random seeds. For each metric, we report the mean and the standard error across runs.

Architectures. For tasks based on the MNIST dataset, we used a feedforward neural network (FFNN) with two hidden layers of 400 units each [21]. All neurons in the hidden and output layers were gain-modulated, where gain represents the slope of the neuron’s input-output response curve. We employed the ReLU activation function and removed all biases. For CIFAR-10 and CIFAR-100,

Table 1: **Main quantitative metrics.** For all benchmarks we report (across tasks) the average final accuracy (avg-ACC), average minimum accuracy (avg-min-ACC), average stability gap drop (avg-SG), and the worst-case accuracy (WC-ACC). We see that our* noradrenergic gain-modulated SGD (NGM-SGD, Equation (1)) exhibits the least stability gaps when encountering a new task and also increases learning efficiency by improving the final learning outcome. Highlighted values indicate the best results; when multiple values are highlighted, it is because their standard error ranges overlap.

		avg-ACC (\uparrow)	avg-min-ACC (\uparrow)	WC-ACC (\uparrow)	avg-SG (\downarrow)
Permuted MNIST	MSGD	92.485 \pm 0.169	50.390 \pm 1.304	64.818 \pm 0.874	0.004 \pm 0.008
	ADAM	93.148 \pm 0.268	51.233 \pm 2.452	65.102 \pm 1.646	0.038 \pm 0.012
	NGM-SGD*	94.186 \pm 0.103	51.697 \pm 1.574	66.022 \pm 1.052	0.011 \pm 0.007
Rotated MNIST	MSGD	93.600 \pm 0.170	48.017 \pm 1.030	63.269 \pm 0.691	0.089 \pm 0.010
	ADAM	92.138 \pm 0.430	48.477 \pm 2.563	62.569 \pm 1.732	0.154 \pm 0.033
	NGM-SGD*	94.948 \pm 0.121	51.006 \pm 1.672	65.536 \pm 1.119	0.054 \pm 0.015
Split MNIST	MSGD	99.085 \pm 0.074	58.083 \pm 3.774	66.148 \pm 3.020	0.270 \pm 0.007
	ADAM	98.602 \pm 0.229	73.255 \pm 9.223	78.082 \pm 7.380	0.155 \pm 0.094
	NGM-SGD*	99.018 \pm 0.055	83.421 \pm 2.840	86.374 \pm 2.272	0.019 \pm 0.005
Split CIFAR-10	MSGD	87.479 \pm 1.754	56.611 \pm 6.399	60.697 \pm 5.182	0.343 \pm 0.087
	ADAM	86.996 \pm 1.659	47.415 \pm 5.827	54.317 \pm 4.792	0.495 \pm 0.100
	NGM-SGD*	90.096 \pm 1.087	63.875 \pm 3.660	67.650 \pm 3.017	0.157 \pm 0.041
Domain CIFAR-100	MSGD	48.600 \pm 1.993	6.470 \pm 3.092	19.980 \pm 2.363	0.579 \pm 0.095
	ADAM	44.713 \pm 0.858	10.000 \pm 0.000	21.520 \pm 0.199	0.872 \pm 0.056
	NGM-SGD*	47.682 \pm 1.527	12.400 \pm 1.375	23.462 \pm 1.381	0.466 \pm 0.061

the increased visual complexity motivated the use of convolutional layers, so we adopted a Slim ResNet-18 backbone [15], [21]. Convolutional networks mirror the brain’s hierarchy of feature detectors, but unlike biological neurons where each has its own input-output curve, CNN feature maps use a shared filter, so uniform scaling cannot match sensitivity at the neuron-level and may disrupt useful feature learning. Thus, we restricted gain modulation to the output layer³, where it could regulate input sensitivity without disrupting feature selectivity, consistent with biological neurons [18]. This choice is also supported by findings that link the output layer to the stability gap phenomenon [35].

Optimization. MSGD [1] optimization used SGD with 0.9 momentum, Adam [13] optimization used betas 0.9 and 0.99 for all experiments. NGM-SGD optimization followed Equation (1) with a decay rate (γ) of 0.9 and scale factors (η) of 0.3, 0.5, 0.4, 0.2, 0.2 for the experiments on Permuted MNIST, Rotated MNIST, Split MNIST, Split CIFAR-10, and Domain CIFAR-100; respectively. In all experiments and for all optimizers, a learning rate of 0.01 was used. To ensure a fair comparison between optimizers, we train the models in the same manner across all experiments, varying only the optimizer.

4.2 Results

In Table 1, we summarize the main experimental results across benchmarks using standard continual evaluation metrics established early in the field ([21], see Appendix). The final average accuracy (avg-ACC) reflects the model’s overall performance by averaging classification accuracy across all tasks at the end of training [28]. The average minimum accuracy (avg-min-ACC) captures the lowest accuracy reached per task, averaged across tasks [28], and serves as a measure of transient forgetting. The worst-case accuracy (WC-ACC) incorporates the minimum accuracy on prior tasks and the accuracy on the current task, offering a measure of the stability-plasticity trade-off [21], [35]. Lastly, the stability gap (avg-SG) represents the maximum observed drop in accuracy throughout training [27], [35], highlighting how much the model degrades when acquiring new tasks.

NGM-SDG reduces stability gaps. Table 1 shows NGM-SDG consistently reduces the stability gap and generally improves performance, as hypothesized in previous studies [28]. For class-incremental

³In the NGM-SGD cases on Slim Resnet18, we trained the backbone with MSGD to maintain the network’s stability in learning features.

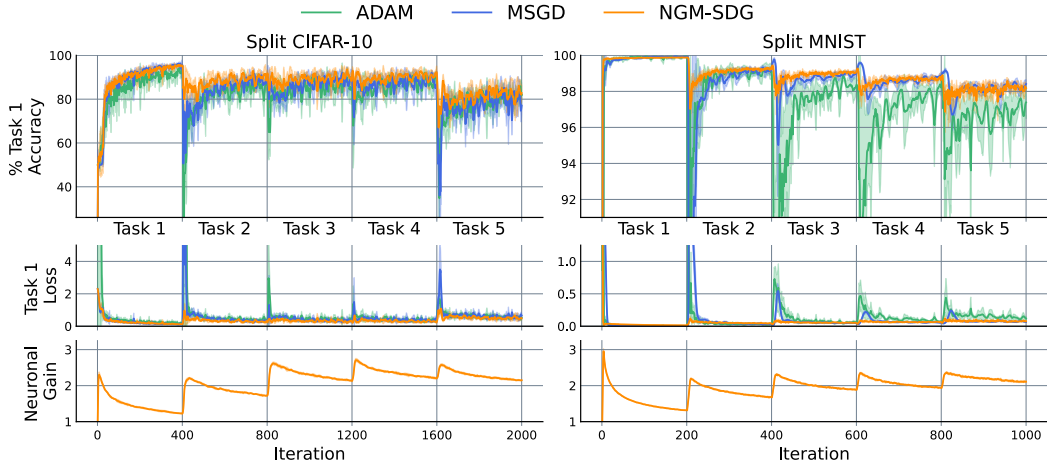


Figure 2: **Stability gaps under class-incremental learning.** The left column shows results on Split CIFAR-10, and the right column on Split MNIST. The top panels display the test accuracy on the first task as the model is incrementally trained on all benchmark tasks. The middle panels show the corresponding test loss, and the bottom panels depict the evolution of neuronal gain across training iterations. Curves represent the mean \pm standard error (shaded area) over five runs with different random seeds. Color coding denotes the different optimizers: our method (NGM-SGD, Equation (1)) in orange, momentum-SGD (MSGD) in blue, and Adam in green. Plots have been zoomed in to better highlight the stability gaps. As a result, some performance drops may appear truncated. Full, unzoomed versions of the plots are provided in the Appendix.

tasks, MSGD and Adam show strong transient forgetting, likely due to increasing task complexity as new classes resemble previously learned ones. NGM-SGD mitigates this by using uncertainty-driven gain to reduce perceived complexity. In Split MNIST, this effect fades as fewer novel classes are introduced in later tasks. In Split CIFAR-10, forgetting is minimal during tasks 2–4, which involve animal classes distinct from the initial vehicle task⁴. However, the final task reintroduces vehicle classes, thus causing interference and a renewed stability gap, which is again attenuated by NGM-SGD. Results in domain-incremental tasks are mixed. NGM-SGD shows clear gains in both performance and stability on Rotated MNIST, and mainly in the first domain of Domain CIFAR-100. In Permuted MNIST, improvements are limited to performance, with a stability gap at the first task switch likely due to a sharp shift in input correlations. Notably, CIFAR results are informative since gain modulation was applied only to the classification head of Resnet18. This supports the findings of Łapacz *et al.* [35], who identified the output layer as the main source of stability gaps.

Gain-boosts reduce test loss at task boundaries. Aiming to understand the origin of the reduction of the stability gaps by the NGM-SGD method, we plotted the first-task loss for each experiment. Figures 2 and 3 show that NGM-SGD systematically reduces the test loss at task transitions compared to ADAM and MSGD. We hypothesize that this behavior comes from the effect of gain increase on flattening the energy landscape [20], [39]. Notably, the learning trajectory followed by NGM-SGD may not correspond to the path of non-increasing loss that recent studies have posited to follow [28], [34], but flattening the energy landscape (here the loss landscape) favors both integration of new information during training of new tasks (see Appendix), while minimizes interference.

Neuronal gain encodes task complexity. In NGM-SGD, neuronal gain evolves according to Equations (4) and (6), rising in response to task-related uncertainty and decaying as learning progresses [39]. As shown in the bottom row of Figures 2 and 3, the asymptotic level to which gain decays differs between class-incremental and domain-incremental settings, reflecting distinct patterns of task complexity (see Appendix). In class-incremental scenarios, gain rises at the beginning of each new task and then decays to a progressively higher baseline. This indicates that the system perceives each new task as increasingly complex, requiring higher sustained sensitivity. In contrast, in domain-incremental tasks, gain also spikes at the onset of each task, but consistently decays to a similar level across tasks. This suggests that most of the complexity is already captured in the first task, and the

⁴Task one consists of two vehicle categories from CIFAR-10 experiments.

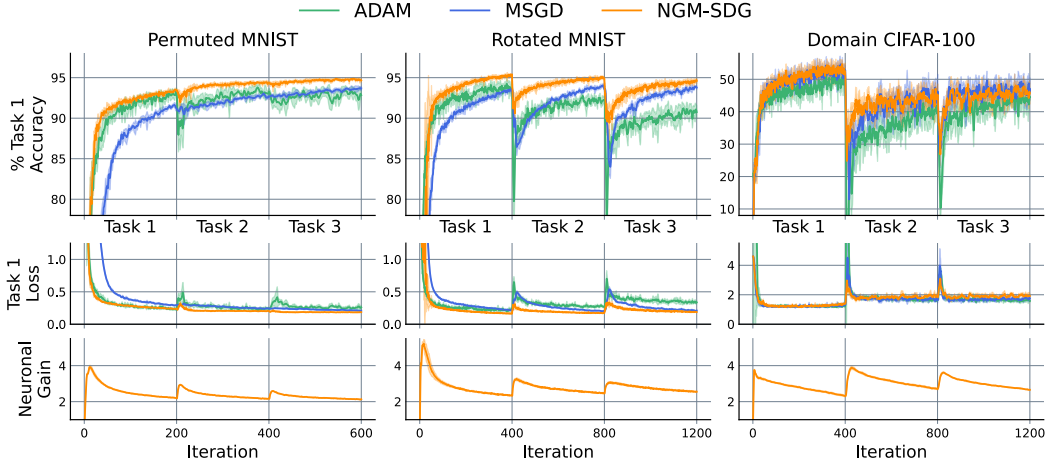


Figure 3: **Stability gaps under domain-incremental learning.** The left column shows results on Permutated MNIST, the middle column on Rotated MNIST with 80° rotations, and the right column on Domain CIFAR-100. The top panels display the test accuracy on the first task as the model is incrementally trained on all benchmark tasks. The middle panels show the corresponding test loss, and the bottom panels depict the evolution of neuronal gain across training iterations. Curves represent the mean \pm standard error (shaded area) over five runs with different random seeds. Color coding denotes the different optimizers: our method (NGM-SGD, Equation (1)) in orange, momentum-SGD (MSGD) in blue, and Adam in green. Plots have been zoomed in to better highlight the stability gaps. As a result, some performance drops may appear truncated. Full, unzoomed versions of the plots are provided in the Appendix.

subsequent tasks do not introduce additional uncertainty. Thus, the long-term gain level serves as a proxy for accumulated task complexity, echoing how biological systems adjust their internal gain to reflect changes in cognitive demand [5], [18].

5 Discussion

A central contribution of our work is the shift in perspective from what to optimize in CL, to how to optimize it [28]. In this context, our work proposes gain modulation as a biologically inspired mechanism to reframe the optimization process. Rather than relying on fixed learning trajectories in a static loss landscape, we introduce uncertainty-driven gain boosts that dynamically reshape the learning dynamics, enabling transient adaptation and long-term retention with minimal interference. This approach draws directly from neurobiological insights, particularly the role of noradrenergic phasic bursts in enhancing cortical responsiveness during moments of uncertainty [5], [17], [33].

Two key effects of gain modulation help explain the observed reduction in stability gaps. First, our analytical and empirical results show that transient gain boosts induce fast and slow timescales of weight adaptation, approximating the fast-and-slow paradigm without explicitly partitioning parameters [2]. This dynamic supports rapid task integration while preserving prior knowledge. Second, consistent with biophysical models [20], [39], we observe that gain increases at task switches flatten the loss landscape, which correlates with reduced test loss and interference, providing a flexible optimization path that mitigates transient forgetting.

Taken together, these results challenge the conventional assumption that optimal learning in continual scenarios must follow a path of monotonically decreasing loss. Instead, our findings suggest that biological systems may rely on mechanisms that dynamically alter the geometry of the loss landscape to accommodate new learning demands. In this view, transient increases in gain, triggered by contextual uncertainty, temporarily reshape the energy surface, creating a corridor for new task representations to be integrated with minimal interference, without disturbing the broader memory structure.

Limitations and future work. This study is conducted in a simplified setting using MNIST and CIFAR benchmarks, and evaluates performance over a relatively small number of tasks. Moreover,

the joint training scenario represents an idealized form of CL that does not reflect the complexities of real-world environments. Future work could explore the role of cholinergic neuromodulation in task segregation by using a gain gating mechanism to transiently silence specific neurons and prevent their updates, thereby introducing gain modulation as a regularization against catastrophic forgetting and, together with gain boosts, guiding gradient updates with minimal interference for more robust continual learning.

References

- [1] D. E. Rumelhart, G. E. Hinton, and R. J. Williams, “Learning internal representations by error propagation,” in *Parallel Distributed Processing*, D. E. Rumelhart and J. L. McClelland, Eds., vol. 1, Cambridge, MA: MIT Press, 1986, pp. 318–362.
- [2] G. E. Hinton and D. C. Plaut, “Using Fast Weights to Deblur Old Memories,” in *Proceedings of the Ninth Annual Conference of the Cognitive Science Society*, Hillsdale, NJ: Erlbaum, 1987, pp. 177–186. [Online]. Available: <http://www.cs.toronto.edu/~fritz/absps/fastweights.pdf>.
- [3] Y. Lecun, L. Bottou, Y. Bengio, and P. Haffner, “Gradient-based learning applied to document recognition,” *Proceedings of the IEEE*, vol. 86, no. 11, pp. 2278–2324, Nov. 1998, ISSN: 00189219. DOI: 10.1109/5.726791. [Online]. Available: <http://ieeexplore.ieee.org/document/726791/> (visited on 05/14/2025).
- [4] N. Qian, “On the momentum term in gradient descent learning algorithms,” en, *Neural Networks*, vol. 12, no. 1, pp. 145–151, Jan. 1999, ISSN: 08936080. DOI: 10.1016/S0893-6080(98)00116-6. [Online]. Available: <https://linkinghub.elsevier.com/retrieve/pii/S0893608098001166> (visited on 05/12/2025).
- [5] G. Aston-Jones and J. D. Cohen, “An Integrative Theory of Locus Coeruleus-Norepinephrine function: Adaptive Gain and Optimal Performance,” en, *Annual Review of Neuroscience*, vol. 28, no. 1, pp. 403–450, Jul. 2005, ISSN: 0147-006X, 1545-4126. DOI: 10.1146/annurev.neuro.28.061604.135709. [Online]. Available: <https://www.annualreviews.org/doi/10.1146/annurev.neuro.28.061604.135709> (visited on 05/14/2025).
- [6] A. Borst, V. L. Flanagan, and H. Sompolinsky, “Adaptation without parameter change: Dynamic gain control in motion detection,” en, *Proceedings of the National Academy of Sciences*, vol. 102, no. 17, pp. 6172–6176, Apr. 2005, ISSN: 0027-8424, 1091-6490. DOI: 10.1073/pnas.0500491102. [Online]. Available: <https://pnas.org/doi/full/10.1073/pnas.0500491102> (visited on 05/12/2025).
- [7] C. D. Swinehart and L. F. Abbott, “Supervised Learning Through Neuronal Response Modulation,” en, *Neural Computation*, vol. 17, no. 3, pp. 609–631, Mar. 2005, ISSN: 0899-7667, 1530-888X. DOI: 10.1162/0899766053019980. [Online]. Available: <https://direct.mit.edu/neco/article/17/3/609-631/6929> (visited on 05/12/2025).
- [8] A. J. Yu and P. Dayan, “Uncertainty, Neuromodulation, and Attention,” en, *Neuron*, vol. 46, no. 4, pp. 681–692, May 2005, ISSN: 08966273. DOI: 10.1016/j.neuron.2005.04.026. [Online]. Available: <https://linkinghub.elsevier.com/retrieve/pii/S0896627305003624> (visited on 05/13/2025).
- [9] P. Dayan and A. J. Yu, “Phasic norepinephrine: A neural interrupt signal for unexpected events,” en, *Network: Computation in Neural Systems*, vol. 17, no. 4, pp. 335–350, Jan. 2006, ISSN: 0954-898X, 1361-6536. DOI: 10.1080/09548980601004024. [Online]. Available: <https://www.tandfonline.com/doi/full/10.1080/09548980601004024> (visited on 05/13/2025).
- [10] S. Hong, B. N. Lundstrom, and A. L. Fairhall, “Intrinsic Gain Modulation and Adaptive Neural Coding,” en, *PLoS Computational Biology*, vol. 4, no. 7, K. J. Friston, Ed., e1000119, Jul. 2008, ISSN: 1553-7358. DOI: 10.1371/journal.pcbi.1000119. [Online]. Available: <https://dx.plos.org/10.1371/journal.pcbi.1000119> (visited on 05/12/2025).
- [11] A. Krizhevsky and G. Hinton, “Learning Multiple Layers of Features from Tiny Images,” en, Ph.D. dissertation, University of Toronto, 2009.
- [12] I. J. Goodfellow, M. Mirza, D. Xiao, A. Courville, and Y. Bengio, *An Empirical Investigation of Catastrophic Forgetting in Gradient-Based Neural Networks*, Version Number: 3, 2013. DOI: 10.48550/ARXIV.1312.6211. [Online]. Available: <https://arxiv.org/abs/1312.6211> (visited on 05/14/2025).

- [13] D. P. Kingma and J. Ba, *Adam: A Method for Stochastic Optimization*, Version Number: 9, 2014. DOI: 10.48550/ARXIV.1412.6980. [Online]. Available: <https://arxiv.org/abs/1412.6980> (visited on 05/12/2025).
- [14] L. C. Garcia Del Molino, G. R. Yang, J. F. Mejias, and X.-J. Wang, “Paradoxical response reversal of top-down modulation in cortical circuits with three interneuron types,” en, *eLife*, vol. 6, e29742, Dec. 2017, ISSN: 2050-084X. DOI: 10.7554/eLife.29742. [Online]. Available: <https://elifesciences.org/articles/29742> (visited on 05/12/2025).
- [15] D. Lopez-Paz and M. Ranzato, *Gradient Episodic Memory for Continual Learning*, Version Number: 6, 2017. DOI: 10.48550/ARXIV.1706.08840. [Online]. Available: <https://arxiv.org/abs/1706.08840> (visited on 05/14/2025).
- [16] J. P. Stroud, M. A. Porter, G. Hennequin, and T. P. Vogels, “Motor primitives in space and time via targeted gain modulation in cortical networks,” en, *Nature Neuroscience*, vol. 21, no. 12, pp. 1774–1783, Dec. 2018, ISSN: 1097-6256, 1546-1726. DOI: 10.1038/s41593-018-0276-0. [Online]. Available: <https://www.nature.com/articles/s41593-018-0276-0> (visited on 05/12/2025).
- [17] J. M. Shine, “Neuromodulatory Influences on Integration and Segregation in the Brain,” en, *Trends in Cognitive Sciences*, vol. 23, no. 7, pp. 572–583, Jul. 2019, ISSN: 13646613. DOI: 10.1016/j.tics.2019.04.002. [Online]. Available: <https://linkinghub.elsevier.com/retrieve/pii/S1364661319300944> (visited on 05/08/2025).
- [18] K. A. Ferguson and J. A. Cardin, “Mechanisms underlying gain modulation in the cortex,” en, *Nature Reviews Neuroscience*, vol. 21, no. 2, pp. 80–92, Feb. 2020, ISSN: 1471-003X, 1471-0048. DOI: 10.1038/s41583-019-0253-y. [Online]. Available: <https://www.nature.com/articles/s41583-019-0253-y> (visited on 04/21/2025).
- [19] L. Caccia, R. Aljundi, N. Asadi, T. Tuytelaars, J. Pineau, and E. Belilovsky, *New Insights on Reducing Abrupt Representation Change in Online Continual Learning*, Version Number: 3, 2021. DOI: 10.48550/ARXIV.2104.05025. [Online]. Available: <https://arxiv.org/abs/2104.05025> (visited on 05/12/2025).
- [20] B. R. Munn, E. J. Müller, G. Wainstein, and J. M. Shine, “The ascending arousal system shapes neural dynamics to mediate awareness of cognitive states,” en, *Nature Communications*, vol. 12, no. 1, p. 6016, Oct. 2021, ISSN: 2041-1723. DOI: 10.1038/s41467-021-26268-x. [Online]. Available: <https://www.nature.com/articles/s41467-021-26268-x> (visited on 05/12/2025).
- [21] M. De Lange, G. van de Ven, and T. Tuytelaars, *Continual evaluation for lifelong learning: Identifying the stability gap*, Version Number: 2, 2022. DOI: 10.48550/ARXIV.2205.13452. [Online]. Available: <https://arxiv.org/abs/2205.13452> (visited on 05/12/2025).
- [22] M. Jones, “Learning at multiple timescales,” in *NeurIPS Workshop on Memory in Artificial and Real Intelligence (MemARI)*, 2022.
- [23] D. Kudithipudi, M. Aguilar-Simon, J. Babb, *et al.*, “Biological underpinnings for lifelong learning machines,” en, *Nature Machine Intelligence*, vol. 4, no. 3, pp. 196–210, Mar. 2022, ISSN: 2522-5839. DOI: 10.1038/s42256-022-00452-0. [Online]. Available: <https://www.nature.com/articles/s42256-022-00452-0> (visited on 05/08/2025).
- [24] G. M. Van De Ven, T. Tuytelaars, and A. S. Tolias, “Three types of incremental learning,” en, *Nature Machine Intelligence*, vol. 4, no. 12, pp. 1185–1197, Dec. 2022, ISSN: 2522-5839. DOI: 10.1038/s42256-022-00568-3. [Online]. Available: <https://www.nature.com/articles/s42256-022-00568-3> (visited on 04/21/2025).
- [25] L. R. Duong, D. Lipshutz, D. J. Heeger, D. B. Chklovskii, and E. P. Simoncelli, “Adaptive whitening in neural populations with gain-modulating interneurons,” 2023, Publisher: arXiv Version Number: 2. DOI: 10.48550/ARXIV.2301.11955. [Online]. Available: <https://arxiv.org/abs/2301.11955> (visited on 05/12/2025).
- [26] L. R. Duong, E. P. Simoncelli, D. B. Chklovskii, and D. Lipshutz, *Adaptive whitening with fast gain modulation and slow synaptic plasticity*, Version Number: 2, 2023. DOI: 10.48550/ARXIV.2308.13633. [Online]. Available: <https://arxiv.org/abs/2308.13633> (visited on 04/21/2025).
- [27] M. Y. Harun and C. Kanan, *Overcoming the Stability Gap in Continual Learning*, Version Number: 4, 2023. DOI: 10.48550/ARXIV.2306.01904. [Online]. Available: <https://arxiv.org/abs/2306.01904> (visited on 05/12/2025).

- [28] T. Hess, T. Tuytelaars, and G. M. van de Ven, “Two Complementary Perspectives to Continual Learning: Ask Not Only What to Optimize, But Also How,” 2023, Publisher: arXiv Version Number: 2. DOI: 10.48550/ARXIV.2311.04898. [Online]. Available: <https://arxiv.org/abs/2311.04898> (visited on 05/12/2025).
- [29] B. R. Munn, E. J. Müller, V. Medel, *et al.*, “Neuronal connected burst cascades bridge macroscale adaptive signatures across arousal states,” en, *Nature Communications*, vol. 14, no. 1, p. 6846, Oct. 2023, ISSN: 2041-1723. DOI: 10.1038/s41467-023-42465-2. [Online]. Available: <https://www.nature.com/articles/s41467-023-42465-2> (visited on 05/12/2025).
- [30] A. Soutif-Cormerais, A. Carta, and J. Van de Weijer, *Improving Online Continual Learning Performance and Stability with Temporal Ensembles*, Version Number: 2, 2023. DOI: 10.48550/ARXIV.2306.16817. [Online]. Available: <https://arxiv.org/abs/2306.16817> (visited on 05/12/2025).
- [31] C. J. Whyte, E. J. Müller, J. Aru, *et al.*, *A Burst-dependent Thalamocortical Substrate for Perceptual Awareness*, en, Jul. 2023. DOI: 10.1101/2023.07.13.548934. [Online]. Available: <http://biorxiv.org/lookup/doi/10.1101/2023.07.13.548934> (visited on 05/12/2025).
- [32] Y. Guo, J. Fu, H. Zhang, D. Zhao, and Y. Shen, *Efficient Continual Pre-training by Mitigating the Stability Gap*, Version Number: 2, 2024. DOI: 10.48550/ARXIV.2406.14833. [Online]. Available: <https://arxiv.org/abs/2406.14833> (visited on 05/12/2025).
- [33] R. Jordan, “The locus coeruleus as a global model failure system,” en, *Trends in Neurosciences*, vol. 47, no. 2, pp. 92–105, Feb. 2024, ISSN: 01662236. DOI: 10.1016/j.tins.2023.11.006. [Online]. Available: <https://linkinghub.elsevier.com/retrieve/pii/S0166223623002680> (visited on 04/21/2025).
- [34] S. Kamath, A. Soutif-Cormerais, J. van de Weijer, and B. Raducanu, *The Expanding Scope of the Stability Gap: Unveiling its Presence in Joint Incremental Learning of Homogeneous Tasks*, Version Number: 1, 2024. DOI: 10.48550/ARXIV.2406.05114. [Online]. Available: <https://arxiv.org/abs/2406.05114> (visited on 05/12/2025).
- [35] W. Łapacz, D. Marczak, F. Szatkowski, and T. Trzciński, *Exploring the Stability Gap in Continual Learning: The Role of the Classification Head*, Version Number: 2, 2024. DOI: 10.48550/ARXIV.2411.04723. [Online]. Available: <https://arxiv.org/abs/2411.04723> (visited on 05/12/2025).
- [36] A. Rodriguez-Garcia, J. Mei, and S. Ramaswamy, *Enhancing learning in spiking neural networks through neuronal heterogeneity and neuromodulatory signaling*, Version Number: 4, 2024. DOI: 10.48550/ARXIV.2407.04525. [Online]. Available: <https://arxiv.org/abs/2407.04525> (visited on 05/12/2025).
- [37] H. Bos, C. Miehl, A.-M. M. Oswald, and B. Doiron, “Untangling stability and gain modulation in cortical circuits with multiple interneuron classes,” en, *eLife*, vol. 13, RP99808, Apr. 2025, ISSN: 2050-084X. DOI: 10.7554/eLife.99808. [Online]. Available: <https://elifesciences.org/articles/99808> (visited on 05/12/2025).
- [38] J. Mei, A. Rodriguez-Garcia, D. Takeuchi, *et al.*, *Improving the adaptive and continuous learning capabilities of artificial neural networks: Lessons from multi-neuromodulatory dynamics*, Version Number: 1, 2025. DOI: 10.48550/ARXIV.2501.06762. [Online]. Available: <https://arxiv.org/abs/2501.06762> (visited on 05/12/2025).
- [39] G. Wainstein, C. J. Whyte, K. A. E. Martens, *et al.*, *Gain neuromodulation mediates task-relevant perceptual switches: Evidence from pupillometry, fMRI, and RNN Modelling*, Feb. 2025. DOI: 10.7554/eLife.93191.2. [Online]. Available: <https://elifesciences.org/reviewed-preprints/93191v2> (visited on 04/21/2025).
- [40] Caroline Haimerl, Eero Simoncelli, and Cristina Savin, *Fine-tuning hierarchical circuits through learned stochastic co-modulation*, en. DOI: 10.57736/WW-E49B-6195. [Online]. Available: <https://www.world-wide.org/cosyne-22/finetuning-hierarchical-circuits-through-2cf75432> (visited on 05/12/2025).

APPENDIX

The Appendix contains additional information for the content presented in the main body. Appendix A derives the continuous-time form of our gain update (Equation (4)), casting the discrete-time rule into a physiologically interpretable differential equation. Appendix B provides full reproducibility details, including model architectures, training hyperparameters, dataset splits, and computing environment. Appendix C defines the evaluation metrics (average accuracy, stability gaps, worst-case accuracy) used to quantify continual-learning performance. Finally, Appendix D presents additional experiments and analyses omitted from the main text – training curves (Figure S1), gain-uncertainty and task-complexity trends (Figure S2), and full-range stability-gap comparisons (Figure S3 and S4).

A Continuous-time gain

We will derive the continuous-time form of the gain update starting from Equation (4). First, we subtract $g(t)$ from both sides, i.e.

$$\begin{aligned} g(t+1) - g(t) &= \gamma g(t) + (1 - \gamma)g_0 + \alpha H(y) - g(t) \\ &= (\gamma - 1) g(t) + (1 - \gamma)g_0 + \alpha H(y) \\ &= (1 - \gamma) (g_0 - g(t)) + \alpha H(y). \end{aligned}$$

Next, dividing both sides by the discrete time interval Δt , we obtain

$$\frac{g(t+1) - g(t)}{\Delta t} = \frac{(1 - \gamma)}{\Delta t} (g_0 - g(t)) + \frac{\alpha}{\Delta t} H(y).$$

Considering Euler’s method for numerical integration and defining the characteristic time constant $\tau = \Delta t / (1 - \gamma)$, and the coefficient $\kappa = (\alpha / \Delta t) \tau = \alpha / (1 - \gamma)$, we arrive at the continuous-time differential equation

$$\tau \frac{dg(t)}{dt} = (g_0 - g(t)) + \kappa H(y) \tag{7}$$

which describes a dynamic evolution reminiscent of increased arousal mediated by noradrenergic release from the locus coeruleus. This type of modulation is similarly observed in physiological responses, such as pupil dilation accompanying perceptual shifts and unexpected stimuli [39].

B Reproducibility details

For all experiments and optimizers, the learning rate was fixed at 0.01, and only weight parameters were updated (all biases were omitted) in every MLP unit; the baseline gain g_0 was set to 1 throughout. MSGD was implemented as SGD with momentum 0.9, and Adam used $\beta_1 = 0.9$, $\beta_2 = 0.99$. To ensure a fair comparison, all other aspects of model training were held constant, varying only the choice of optimizer.

Class-incremental experiments. We evaluated class-incremental learning on two benchmarks: Split MNIST and Split CIFAR-10. For Split MNIST, we used an FFNN with two hidden layers of 400 units each and a 10-unit output layer, applying gain modulation to all hidden and output neurons. The dataset was divided into five sequential tasks of two classes each, starting with classes {0,1} and then adding {2,3}, {4,5}, {6,7}, and {8,9}, retaining previously learned classes throughout joint training. Models were trained with a mini-batch size of 128 for 200 iterations per task, sampling uniformly at random, and evaluated on the full test set of the first task’s classes. NGM-SGD was run with gain-decay $\gamma = 0.9$ and entropy scale $\eta = 0.4$. For Split CIFAR-10, we adopted a slim ResNet-18 backbone with gain modulation restricted to the 10-unit output layer. CIFAR-10 was partitioned into five tasks of two classes each – {*airplane, automobile*}, {*bird, cat*}, {*deer, dog*}, {*frog, horse*}, and {*ship, truck*} – in sequence, retaining prior classes under joint training. Training used mini-batch size 256 for 400 iterations per task, with uniform random sampling; testing was performed on all test samples of {*airplane, automobile*}. NGM-SGD employed $\gamma = 0.9$, $\eta = 0.2$, and the ResNet-18 backbone was optimized with momentum-SGD (momentum 0.9).

Domain-incremental experiments. We evaluated domain-incremental learning on three benchmarks: Permuted MNIST, Rotated MNIST, and Domain CIFAR-100. For Permuted MNIST, we used an FFNN with two hidden layers of 400 units each and a 10-unit output layer, with gain modulation on all neurons. Task 1 was standard MNIST classification, and subsequent tasks applied fixed random pixel permutations, trained jointly while retaining prior tasks. Models were trained with a mini-batch size of 128 for 200 iterations per task (uniform random sampling), and evaluated on the full original MNIST test set. NGM-SGD used gain-decay $\gamma = 0.9$ and entropy scale $\eta = 0.3$. For Rotated MNIST, again, we used the 2×400 -unit FFNN with gain on every neuronal unit. Task 1 was unaltered MNIST, followed by two rotation tasks at $\phi = 80^\circ$, trained jointly. Training used mini-batch size 128 for 400 iterations per task (uniform sampling); testing was on the original MNIST test set. NGM-SGD employed $\gamma = 0.9$ and $\eta = 0.5$. For Domain CIFAR-100, we adopted a slim ResNet-18 backbone with gain modulation on the 100-unit output layer. Task 1 was the *aquatic mammals* superclass (5 classes), followed by *fish* and *flowers* superclasses (5 classes each), trained jointly. Models were trained with a mini-batch size of 256 for 400 iterations per task (uniform sampling) and were evaluated on the *aquatic mammals* test set. NGM-SGD used $\gamma = 0.9$, $\eta = 0.2$, while the ResNet-18 backbone was optimized with momentum-SGD (momentum 0.9).

Code availability. To enable the reproduction of all experiments, the relevant code will be made openly accessible. For the review process, it is provided in the zipped file.

Computer resources. All experiments were run on a system with an Intel Core i9-14900K CPU (8 P-cores @ 3.2–6.0 GHz, 16 E-cores @ 2.4–4.4 GHz; 32 threads), 64 GB DDR5-4800 MHz RAM (2x32 GB, CL40) and a PNY NVIDIA RTX 4000 Ada Lovelace GPU (20 GB GDDR6). Code was implemented using Python 3.10.16 in PyTorch 2.5.1 with CUDA 11.8.

C Evaluation metrics

Throughout this work, we quantify model performance using **classification accuracy**, the percentage of correctly predicted labels on a test set. Formally, for the testing dataset D and model F_θ , we denote the classification accuracy $\mathbf{A}(D, F_\theta)$ as the percentage of samples in D that are correctly classified by F_θ . In practice, we evaluate on the full test set for the first task, although a reduced evaluation set of 1,000 examples per task, sampled uniformly at random in each run, has been shown to closely approximate the full-set results [21], [28].

Final average accuracy. We further define the final average accuracy as the classification accuracy averaged over all contexts at the end of training. Formally, consider a continual-learning sequence of K contexts (tasks). Let $F_{\theta_t}^{(k)}$ denote the model parameters immediately after training on context k , and let D_k be its corresponding held-out test set. Hence, we define

$$\mathbf{avg-ACC} = \frac{1}{K} \sum_{k=1}^K \mathbf{A}(D_k, F_{\theta_t}^{(k)}).$$

This metric captures overall end-of-sequence performance but does not reflect transient drops in accuracy that may occur during intermediate stages of training.

Average minimum accuracy. To assess worst-case retention within each context, we track the lowest classification accuracies observed for each context and define the average minimum accuracy as the average of these minimum accuracies. Formally, with I_C be the set of training-iteration indices following completion of context k , we have

$$\mathbf{avg-min-ACC} = \frac{1}{K-1} \sum_{k=1}^{K-1} \min_{i \in I_C} \mathbf{A}(D_k, F_{\theta_i}^{(k)}),$$

where $F_{\theta_i}^{(k)}$ indicates the model at the i -th training iteration in context k .

Worst-case accuracy. To capture the balance between plasticity (learning the most recent task) and stability (preserving earlier tasks) [26], [35], we define worst-case accuracy as

$$\mathbf{WC-ACC} = \frac{1}{K} \mathbf{A}(D_k, F_{\theta_t}^{(k)}) + \left(1 - \frac{1}{K}\right) \mathbf{avg-min-ACC}.$$

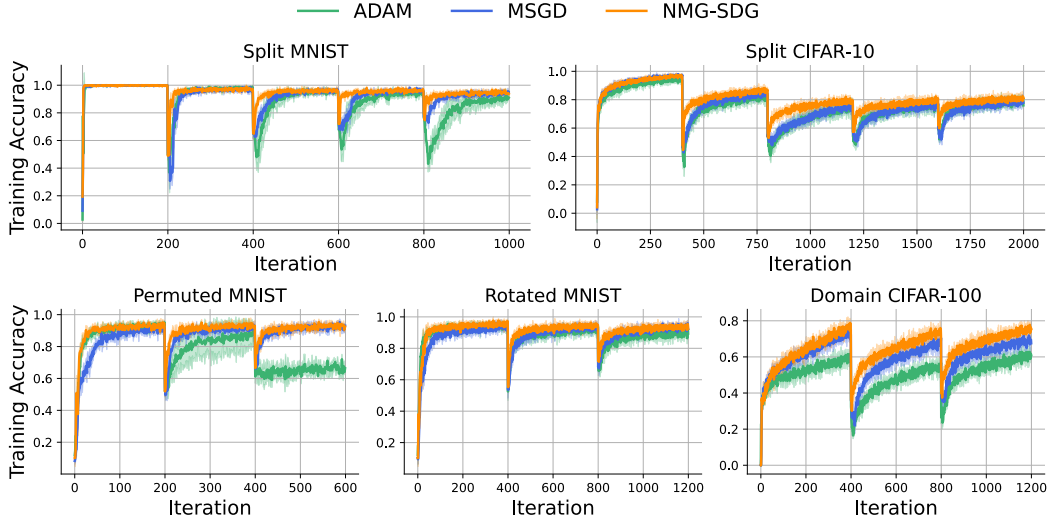


Figure S1: **Training accuracy across tasks.** The top row shows class-incremental learning results on Split MNIST (left) and CIFAR-10 (right). The bottom row shows domain-incremental learning results on Permuted MNIST (left), Rotated MNIST (middle) and Domain CIFAR-100 (right). Curves represent the mean \pm standard error in the shaded region over five runs with different random seeds. Colors denote the optimizers NMG-SGD in orange, MSGD in blue and Adam in green.

Hence, a high **WC-ACC** indicates both effective adaptation to new tasks and minimal forgetting of prior tasks. Note that we are evaluating this at the end of the experiment, but it can also be considered at each iteration.

Average stability gap. We define the average stability gap as the mean relative drop in classification accuracy that occurs when shifting from one context to the next [35]. For a sequence of K contexts, the stability gap at the transition from context $k - 1$ to context k is given by

$$\mathbf{SG}_k = \frac{\mathbf{A}(D_{k-1}, F_{\theta_t}^{(k-1)}) - \min_{i \in I_C} \mathbf{A}(D_k, F_{\theta_i}^{(k)})}{\mathbf{A}(D_{k-1}, F_{\theta_t}^{(k-1)})},$$

and the average stability gap is then:

$$\mathbf{avg-SG} = \frac{1}{K - 1} \sum_{k=2}^K \mathbf{SG}_k.$$

By normalizing each drop by the accuracy just before the transition, we ensure that stability gaps are directly comparable even when baseline performance differs across tasks. A large **avg-SG** signals that the model experiences significant forgetting immediately after each context switch, underscoring its lack of robustness in continual learning settings.

D Supporting results

In this section, we present additional results from our experimental protocol that were omitted from the main text for brevity. We begin by examining the accuracy trends observed during training, then showcase the gain-uncertainty and task-complexity analyses, and finally provide the full-scale (unzoomed) stability gap plots for comprehensive comparison.

D.1 Accuracy during training

Theoretical work suggests that transient gain-boosts flatten the energy (loss) landscape, thereby facilitating knowledge acquisition. [20], [29], [39]. Consistent with this, Figure S1 shows that NMG-SGD (orange) sustains higher training accuracy across tasks and exhibits markedly smaller

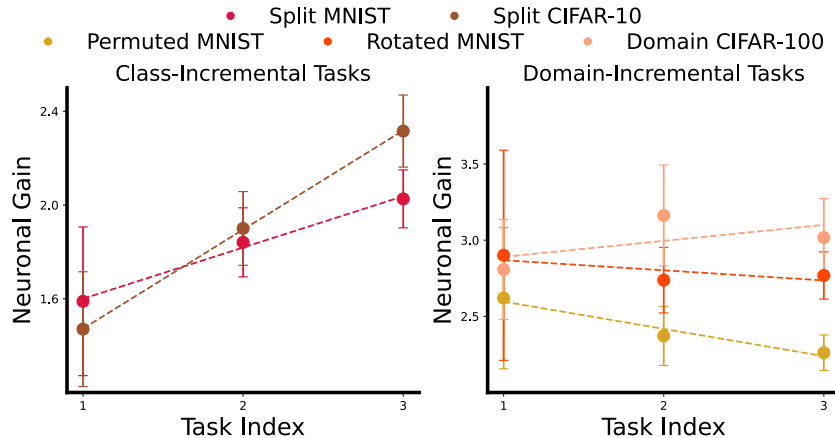


Figure S2: **Gain across tasks.** Plots of the mean neuronal gain in the first 3 tasks for class-incremental (left) and domain-incremental (right) experiments. We used a linear fit and obtained the slopes 0.22 for Split MNIST, 0.42 for Split CIFAR-10, -0.18 for Permuted MNIST, -0.07 for Rotated MNIST, and 0.10 for Domain CIFAR-100.

dips and much faster recoveries at task transitions compared to MSGD (blue) and Adam (green). Biological evidence further supports these findings, in which noradrenergic neuromodulation provides a “network reset”, prompting rapid corrections to predictions on contextual mismatches [17], [33]. However, our stability-gap analysis reveals that noradrenergic gain modulation enables the optimizer to incorporate new-task gradients with a smaller impact on previously learned representations. This suggests that gain-driven flattening of the loss landscape not only accelerates the integration of new information but also minimizes interference with previously acquired representations.

D.2 Gain-uncertainty and task complexity

To explore whether neuronal gain reflects task complexity, we computed the mean gain across the first three tasks in both class-incremental and domain-incremental settings and fitted a linear trend (Figure S2). Since in class-incremental scenarios the novelty added by Tasks 4 and 5 is relatively smaller, we focus on the first three tasks, where changes in complexity are most pronounced.

As shown in Figure S2, the slopes for Split MNIST and Split CIFAR-10 are positive, consistent with the idea that increased task complexity drives up sustained gain. By contrast, Permuted MNIST, Rotated MNIST, and Domain CIFAR-100 exhibit near-zero or slightly negative slopes, indicating little to no increase in complexity across tasks. These patterns suggest that neuronal gain may serve as a proxy for task uncertainty and complexity, in line with evidence that biological systems adjust internal gain to match changing cognitive demands [5], [18].

D.3 Unzoomed stability gap plots

Full-scale (unzoomed) plots (Figures S3 and S4) are provided to offer a comprehensive comparison of stability gaps across optimizers. These complete views reveal the true extent of the performance drops that MSGD and Adam undergo at task transitions and distribution shifts.

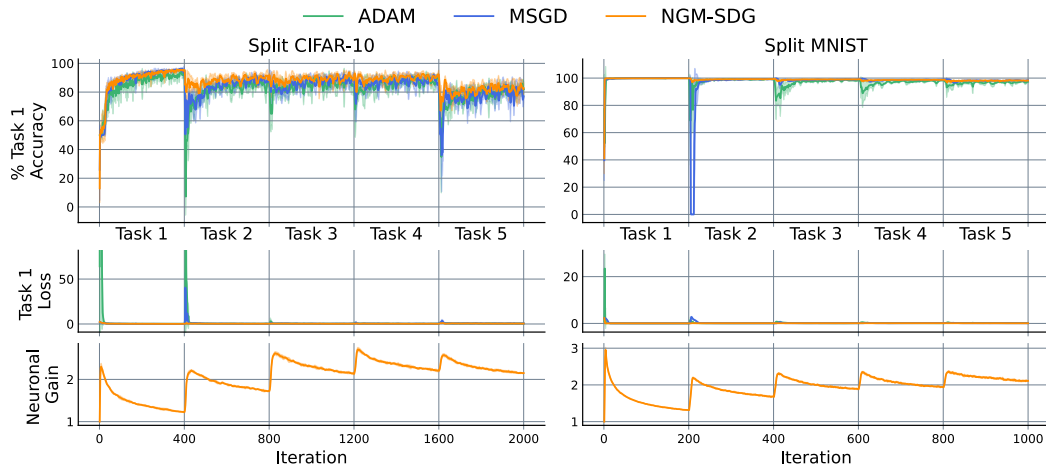


Figure S3: Full-scale training accuracy curves for class-incremental learning on Split MNIST (left) and Split CIFAR-10 (right). The unzoned view highlights the raw stability gaps experienced by each optimizer—NGM-SGD (orange), MSGD (blue), and Adam (green) – curves represent the mean \pm standard error (shaded area) over five runs with different random seeds. However, in most cases, the shaded region is not noticeable.

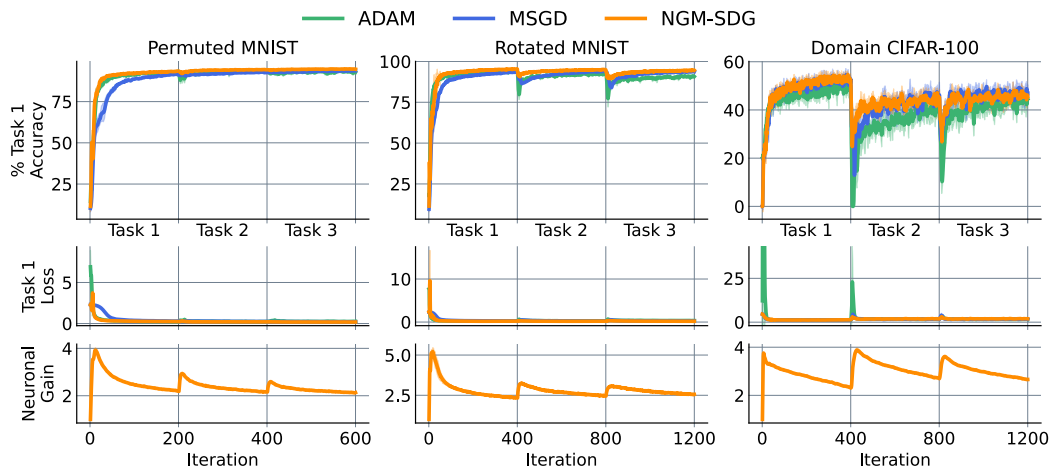


Figure S4: Full-scale training accuracy curves for domain-incremental learning on Permuted MNIST (left), Rotated MNIST (center), and Domain CIFAR-100 (right). These unzoned plots reveal the magnitude of performance drops at task transitions for NGM-SGD (orange), MSGD (blue), and Adam (green) – curves represent the mean \pm standard error (shaded area) over five runs with different random seeds. However, in most cases, the shaded region is not noticeable.